

This work was written as part of one of the author's official duties as an Employee of the United States Government and is therefore a work of the United States Government. In accordance with 17 U.S.C. 105, no copyright protection is available for such works under U.S. Law.

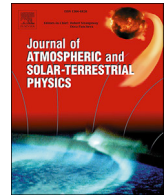
Public Domain Mark 1.0

<https://creativecommons.org/publicdomain/mark/1.0/>

Access to this work was provided by the University of Maryland, Baltimore County (UMBC) ScholarWorks@UMBC digital repository on the Maryland Shared Open Access (MD-SOAR) platform.

Please provide feedback

Please support the ScholarWorks@UMBC repository by emailing scholarworks-group@umbc.edu and telling us what having access to this work means to you and why it's important to you. Thank you.



Solar cycle variations in mesospheric carbon monoxide

Jae N. Lee^{a,*}, Dong L. Wu^b, Alexander Ruzmaikin^c, Juan Fontenla^{d,1}

^a Joint Center for Earth Systems Technology, University of Maryland, Baltimore County, Baltimore, MD, United States

^b NASA Goddard Space Flight Center, Greenbelt, MD, United States

^c Jet Propulsion Laboratory, California Institute of Technology, Pasadena, CA, United States

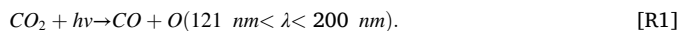
^d GalacTech LLC, Charlotte, SC, United States

ABSTRACT

As an extension of Lee et al. (2013), solar cycle variation of carbon monoxide (CO) is analyzed with MLS observation, which covers more than thirteen years (2004–2017) including maximum of solar cycle 24. Being produced primarily by the carbon dioxide (CO₂) photolysis in the lower thermosphere, the variations of the mesospheric CO concentration are largely driven by the solar cycle modulated ultraviolet (UV) variation. This solar signal extends down to the lower altitudes by the dynamical descent in the winter polar vortex, showing a time lag that is consistent with the average descent velocity. To characterize a global distribution of the solar impact, MLS CO is correlated with the SORCE measured total solar irradiance (TSI) and UV. As high as 0.8 in most of the polar mesosphere, the linear correlation coefficients between CO and UV/TSI are more robust than those found in the previous work. The photochemical contribution explains most (68%) of the total variance of CO while the dynamical contribution accounts for 21% of the total variance at upper mesosphere. The photochemistry driven CO anomaly signal is extended in the tropics by vertical mixing. The solar cycle signal in CO is further examined with the Whole Atmosphere Community Climate Model (WACCM) 3.5 simulation by implementing two different modeled Spectral Solar Irradiances (SSIs): SRPM 2012 and NRLSSI. The model simulations underestimate the mean CO amount and solar cycle variations of CO, by a factor of 3, compared to those obtained from MLS observation. Different inputs of the solar spectrum have small impacts on CO variation.

1. Introduction

Carbon monoxide (CO) is a good tracer to study global middle atmosphere dynamics and transport due to its strong horizontal and vertical gradients and longer than 30 days of photochemical lifetime (Allen et al., 2000; Minschwaner et al., 2010; Lee et al., 2011). While CO can be produced by the oxidation of methane in the stratosphere, the major source of the upper stratospheric and mesospheric CO is known to be photolysis of carbon dioxide (CO₂) at ultraviolet (UV) wavelengths, 121–200 nm, in the lower thermosphere (Bates and Witherspoon, 1951; Solomon et al., 1985):



Because the solar spectral irradiance (SSI) input varies with wavelength and atmospheric opacity, the photolysis processes become a strong function of altitude. The CO₂ photolysis intensity is also a function of CO₂ cross-section. According to the modeled CO₂ absorption cross-section, the photo-dissociation takes place most effectively at the solar Lyman α (121.6 nm) and Schumann-Runge band (175 nm - 200 nm) region, and these processes occur mostly at high altitudes (Solomon et al., 1985; Brasseur and Solomon, 2005; Minschwaner et al., 2010).

As evaluated with Microwave Limb Sounder (MLS) and Atmospheric Chemistry Experiment-Fourier Transform Spectrometer (ACE-FTS) measurements, the CO₂ photo-dissociation rate maximizes at far ultraviolet (FUV), near 145 nm, in the thermosphere (Minschwaner et al., 2010). The photo-dissociation also occurs at wavelengths greater than 175 nm where the O₂ Schumann-Runge bands contribute to the atmospheric opacity. In their calculation of the photo-dissociation rate, Solar Ultraviolet Spectral Irradiance Monitor (SUSIM) measured solar ultraviolet irradiances are used. Different from those estimated by the satellite measurements, the laboratory measurements indicate that the absorption cross-sections of CO₂ are maximum near 135–145 nm (Yoshino et al., 1996; Parkinson et al., 2003).

In addition to photolysis by UV, there are two more sources in the thermosphere; the photolysis of CO₂ at extreme ultraviolet (EUV) and the reaction of CO₂ with the atomic oxygen ion:



The CO production rates via [R2] and [R3] are negligible compared to [R1], below 0.001 hPa (~100 km), but they are major source mechanism

* Corresponding author.

E-mail address: jae.n.lee@nasa.gov (J.N. Lee).

¹ Deceased on January 11, 2018. We dedicate this paper to Dr. Juan Fontenla for his semi-empirical modeling of the Sun.

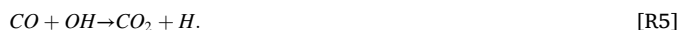
in the lower thermosphere above that level (Garcia et al., 2014).

A major chemical loss of CO above ~ 100 km is due to a three-body recombination with atomic oxygen:



However, this loss reaction is not effective, since photochemical time of this reaction at these altitudes is much slower than the time scale of transport.

CO is also produced by methane oxidation (not shown). During polar night when little OH is present for months, this can be an additional CO source. In the upper stratosphere and mesosphere, CO is rapidly destroyed by the OH oxidation where OH is present (Ryan et al., 2018):



This reaction occurs mostly during the day, when upper-atmospheric OH is produced from photolysis reactions (e.g., with H_2O). Due to low amount of OH in the thermosphere, the chemical loss of the thermospheric CO is negligible and lifetime of CO is long enough to be transported to the mesosphere. Due to lack of OH oxidation during polar night, in particular, CO volume mixing ratio (VMR) has a long photochemical lifetime and can be used as a dynamic tracer in both day and night.

The abundance in the thermosphere allows the anomalous distribution of CO inside the vortex to be transported over a period of 30 days throughout the descent from the mesosphere to the stratopause (Minschwaner et al., 2010; Lee et al., 2011). The unique combination of CO chemistry and prolonged lifetime also lead to a large vertical gradient with VMR values of ppmv (parts per million by volume) in the mesosphere to values of ppbv (parts per billion per volume) in the low stratosphere. The polar vortex descent brings CO further down to the lower stratosphere, producing strong hemispheric asymmetry in its concentration throughout the middle atmosphere. A simple diagram of CO distribution in the middle atmosphere from photo-chemistry and dynamics is illustrated in Fig. 1. Besides the vertical transport inside the polar vortex, vertical mixing due to tidal and gravity wave breaking (Burrage et al., 1995) brings the CO anomaly in the lower thermosphere down to the mesosphere throughout the globe. CO can also be transported by the winter to summer circulation in the lower thermosphere i.e., upwelling of the mesospheric circulation and the downwelling of the lower thermospheric circulation in the summer high latitudes. Recent study (Qian et al., 2017) suggests the winter to summer circulation in the lower thermosphere, by showing large CO_2 vertical gradients in the summer high latitude region.

It requires accurate and stable measurements of both CO and solar irradiance to quantify solar impacts on the CO photolysis in the upper

atmosphere. Recent advancement of solar irradiance measurements from Solar Radiation and Climate Experiment (SORCE) (Rottman, 2005; Pilewskie et al., 2005) enables us to investigate the response of the photo-chemically produced CO, which can be sensitive to the solar 11-year and shorter term, i.e., 27-day solar rotational variability (Ruzmaikin et al., 2014).

This paper is an extension of early work of Lee et al. (2013), hereafter called Lee13, and utilizes more recent CO observation from the Aura MLS observation (2004–present), which covers the maximum of the solar cycle (SC) 24 (2011–2014). The data also cover the solar minimum of the cycle 23 (2008–2009) and provides unprecedented information on the 11-year solar cycle impacts in middle atmospheric chemistry and dynamics. In this study, we analyze the interannual variations of the mesospheric CO observed by MLS and correlations with total and UV solar irradiance measured by SORCE Total Irradiance Monitor (TIM) and Solar-Stellar Irradiance Comparison Experiment (SOLSTICE).

2. Data and methods

2.1. Data

We use the version 4.2x (V4.2x) of the Aura Microwave Limb Sounder (MLS) data for the daily CO and temperature, gridded for day and night, separately, at each pressure levels from the upper troposphere to the mesopause (316 hPa - 0.001 hPa). The daily fields are zonally averaged onto 43 latitude bins for daytime (ascending) and nighttime (descending) orbits. For daily CO and temperature data, the data acquired from ascending and descending orbits are averaged. Because Aura MLS sampling does not cover the regions poleward of 82°N latitude, we use the daily mean from ascending and descending orbits in latitude bins between 82°N and 82°S for Northern and Southern Hemispheres, respectively.

The typical single-profile precision of MLS V4.2x CO varies from 0.02 ppmv at 100 hPa, 0.2 ppmv at 1 hPa, to 11 ppmv at 0.002 hPa, with vertical resolution of 4 , 3 , and 9 km, respectively (https://mls.jpl.nasa.gov/data/v4-2_data_quality_document.pdf). MLS has a good vertical (9 km) and horizontal resolution (200 km) and single profile precision of 11 ppmv in the upper mesosphere (Pumphrey et al., 2007). MLS temperature in the stratosphere and mesosphere is retrieved primarily from bands near O_2 spectral lines at 118 GHz. The precision of the MLS v4.2x temperature measurement is ± 3.6 K, and the bias is ~ 3 K between 0.01 hPa and 0.001 hPa (https://mls.jpl.nasa.gov/data/v4-2_data_quality_document.pdf).

As shown in the zonal mean CO in section 3, the zonal mean CO has a large meridional gradient in its VMR. This gradient, evident in MLS radiance measurements as well, is not affected by the initial guess used in the retrieval algorithm. There is a significant day-to-day variability in the monthly zonal mean CO, which is included by the standard deviation as shown in section 3. However, random errors in MLS CO are greatly reduced in the monthly zonal mean data.

The observed response of CO to the solar cycle depends on the strength of the spectral variability of the solar irradiance over the solar cycle. Besides SOLSTICE measured UV irradiance, TSI and Lyman α (121.6 nm) irradiance composite (<http://lasp.colorado.edu/lisird/lya/>) (Woods et al., 2000) is used as solar indices as indicators of solar irradiance to be correlated with MLS CO. Because knowledge of SSI with sufficient data record length, consistency, and continuity is required to accurately understand the role of the Sun and solar variability in Earth's climate, solar proxy and solar index are widely used in Sun-Earth studies including climate and solar irradiance modeling. Solar irradiance proxy is defined as a measured or modeled data type that can be used as a substitute for solar spectral irradiances at different specified wavelengths or over a wavelength band, according to the International Organization for Standardization (ISO) report 21348:2007. Solar irradiance index is defined as measured or modeled data type that is an indicator, or expresses an activity level, of solar irradiances and can represent a specified

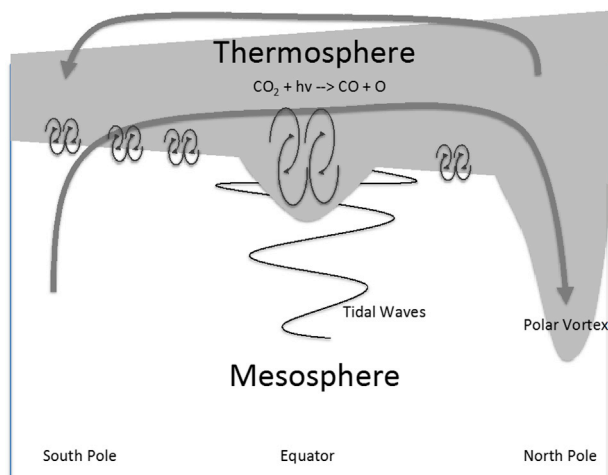


Fig. 1. An illustration of CO distribution in the middle atmosphere, related with photo-chemistry and dynamics.

wavelength or integrated irradiances over a wavelength band.

The TSI data from the SORCE TIM is used in this study as an index, which can indicate solar activity level over the solar cycle. The TIM TSI data have 3 times higher accuracy (0.035%) than previous TSI measurements and with a long-term stability of 0.001% per year (Kopp and Lawrence, 2005; Kopp et al., 2005).

The SORCE SOLSTICE version 11 UV data is also used to find the CO concentration change by the UV modulation. The SOLSTICE measures SSI in UV from 115 to 320 nm with a resolution of 0.1 nm, an absolute accuracy of better than 5%, and a relative accuracy of 0.5% per year (McClintock et al., 2005a, 2005b; Snow et al., 2005). The SOLSTICE measurements are made using a pair of identical spectrometers, SOLSTICE A and SOLSTICE B. Each spectrometer independently makes ultraviolet spectral measurements in two intervals: FUV in 115–180 nm and mid ultraviolet (MUV) in 180–320 nm. With this reason, there are slight discontinuities in the FUV and MUV spectrum near 180 nm region.

2.2. The WACCM simulations

To further study the CO modulation with SSI, we performed Whole Atmosphere Community Climate Model (WACCM) 3.5 simulation experiment with two different solar spectrums, National Research Laboratory Solar Spectral Irradiance (<http://lasp.colorado.edu/lisird/nrlssi/>) (NRLSSI; Lean, 1997, 2000), and Solar Radiation Physical Modeling (SRPM) 2012 (Fontenla et al., 2009, 2011). SRPM 2012 uses solar radiance spectrum for the features observed in images of the solar disk from Meudon (1997–2001) and Rome (2001–2009) observatories. From the imaging data recorded between 2002 and 2008 and the image analysis methods used by SRPM in 2011, the SC 23 SSI was reconstructed and other cycles were simulated from 1955 to 2008 by repeating the 1997–2009 pattern stretched as necessary to match the sunspot minimum times since 1955. NRLSSI reconstructed data was provided as the default in WACCM and reference is thereby provided by WACCM. More information about the simulations can be found in <http://www.digidyna.com/WaccmResults2011/>.

2.3. Statistical significance

To study the CO dependence on the solar cycle forcing, we compute the linear correlation between the MLS CO and SOLSTICE UV data for each latitude and height bin. The statistical significance of the linear correlation coefficients are calculated using a Student's *t* statistic applied to the correlation coefficient *r* with *n** - 2 degrees of freedom:

$$t = r \sqrt{\frac{n^* - 2}{1 - r^2}}$$

The effective sample size *n** is estimated to consider the auto-correlation caused by solar cycle variations, using the *Quenouille's* procedure as described by Angell and Korshover (1981).

3. Results and discussions

3.1. Climatology of CO

MLS observation shows a large vertical gradient in CO VMR, with values from more than 50 ppmv in the winter polar upper mesosphere to ppbv in the low stratosphere (Fig. 2(a) and (c), and 2(e)), confirming its source in the upper atmosphere. CO VMR shows noticeable variation with pressure, latitude, and season.

As seen in Fig. 2(b) and (d), MLS CO VMR in high latitude (62°N/S–82°N/S) show a large annual cycle, in a narrow vertical layer in upper mesosphere, with variation of approximately a factor of 25 between minimum during early summer and maximum during early winter. MLS CO annual cycle shows annual variation from more than 25 ppmv during early winter, and rapidly decrease to near 1 ppmv during polar summer

season in both hemispheres. In the northern hemisphere (NH), CO reaches maximum in November, which is also the month of the strongest solar signal.

CO VMR also shows the Semiannual Oscillation (SAO) signals with secondary peaks in equinox seasons in March, and secondary minima in January. In the southern hemisphere (SH), CO peaks in September with the strongest solar cycle signal (Fig. 2(c)–(d)). The secondary peaks in May and July also show noticeable solar signal, contrary to the transition months post the NH winters. These secondary peaks in the NH and SH are consistent with Michelson Interferometer for Passive Atmospheric Sounding (MIPAS) observations (Funke et al., 2009; Garcia et al., 2014). There is approximately a 6-month phase shift between the annual CO maximum in the NH and SH, while SAO signal is dominant in the tropics. Fig. 2(e)–(f) show a distinct distribution of tropical CO variations in 12 S–12 N, where the predominant SAO amplitudes are nearly equal to those of annual oscillations.

3.2. Solar cycle variation of CO

Besides the seasonal variation, CO VMR also shows a strong inter-annual variation during the analysis period (2004–2017) that correlates with the 11-year solar cycle. In general, the zonal mean CO VMR after 2012 tends to be higher than the values before 2012. Shown in Fig. 3 are interannual variations of high latitude CO VMR at 0.005 hPa, overlaid with SORCE TIM measured TSI data. In the NH high latitude (Fig. 3(a)), the CO amount at 0.005 hPa during early winter varies by about 20%, showing less than 20 ppmv in 2009 when TSI reaches minimum, and more than 25 ppmv when the TSI reaches peak at solar maximum during approximately 2011–2014. Similarly, in the SH high latitude (Fig. 3(b)), CO changes with solar cycle by amount comparable to that in the NH. The solar irradiance variation influence on the photolysis of CO₂, and the modulation of the CO anomaly are transported from the low thermosphere likely play the key role in the wintertime CO distribution.

It is noticeable that the zonal mean CO VMR during the SH early winter is ~10% less than that of the NH. The relatively low amount of CO VMR in the SH winter can be largely caused by the seasonal variation of the Sun–Earth distance. The amount of solar irradiance reaching the Earth in a given period of time depends on the distance between the Earth and the Sun, due to Earth's elliptical orbit. This distance varies by 3.4% during time of the year and the NH receives about 6.8% more solar irradiance during winter, than the SH winter because the Earth is closer to the Sun in January than in July. The solar irradiance variation due to solar geometry influence on the photolysis rate of CO₂, and the CO amount. Therefore the CO, transported from the low thermosphere, is lower in the SH winter than that of NH.

In addition to the hemispheric asymmetry of photolysis caused by ~6.8% of more solar insolation in the NH winter, a large latitude dependence in low thermospheric temperature up to 2% due to this hemispheric imbalance of solar insolation (Waldteufel, 1970; Qian et al., 2009) can enhance the photolysis rate associated with the CO production by increasing absorption cross-section. Similar to the seasonal variation of the mesospheric temperature, as shown in Fig. 8(c) and (d), the MLS temperature shows a large latitudinal variation greater than 50 K, near the mesopause at 0.001 hPa, during the NH winter. The MLS zonal mean temperature in NH high latitude (62°N–82°N) during January is about 5 K warmer than that of July in SH high latitude (62°S–82°S) at that level.

The Improved Stratospheric and Mesospheric Sounder (ISAMS) on board the Upper Atmosphere Research Satellite (UARS) observed CO for one year since October 1991. The SC 22 was at its maximum during 1990–1991, and ISAMS took the measurement slightly after the solar maximum. The zonal mean CO VMR measured by ISAMS during January 1991 was ~3.2 ppmv near 60 N at 0.1 hPa (~65 km) (López-Valverde et al., 1996). This ISAMS measured amount is slightly higher than CO amount measured by Aura MLS during maximum of SC 24 in January of 2012 and 2013 (~2 ppmv) but comparable with the CO measured during February of 2012 and 2013 (~3.1 ppmv), at the similar height and

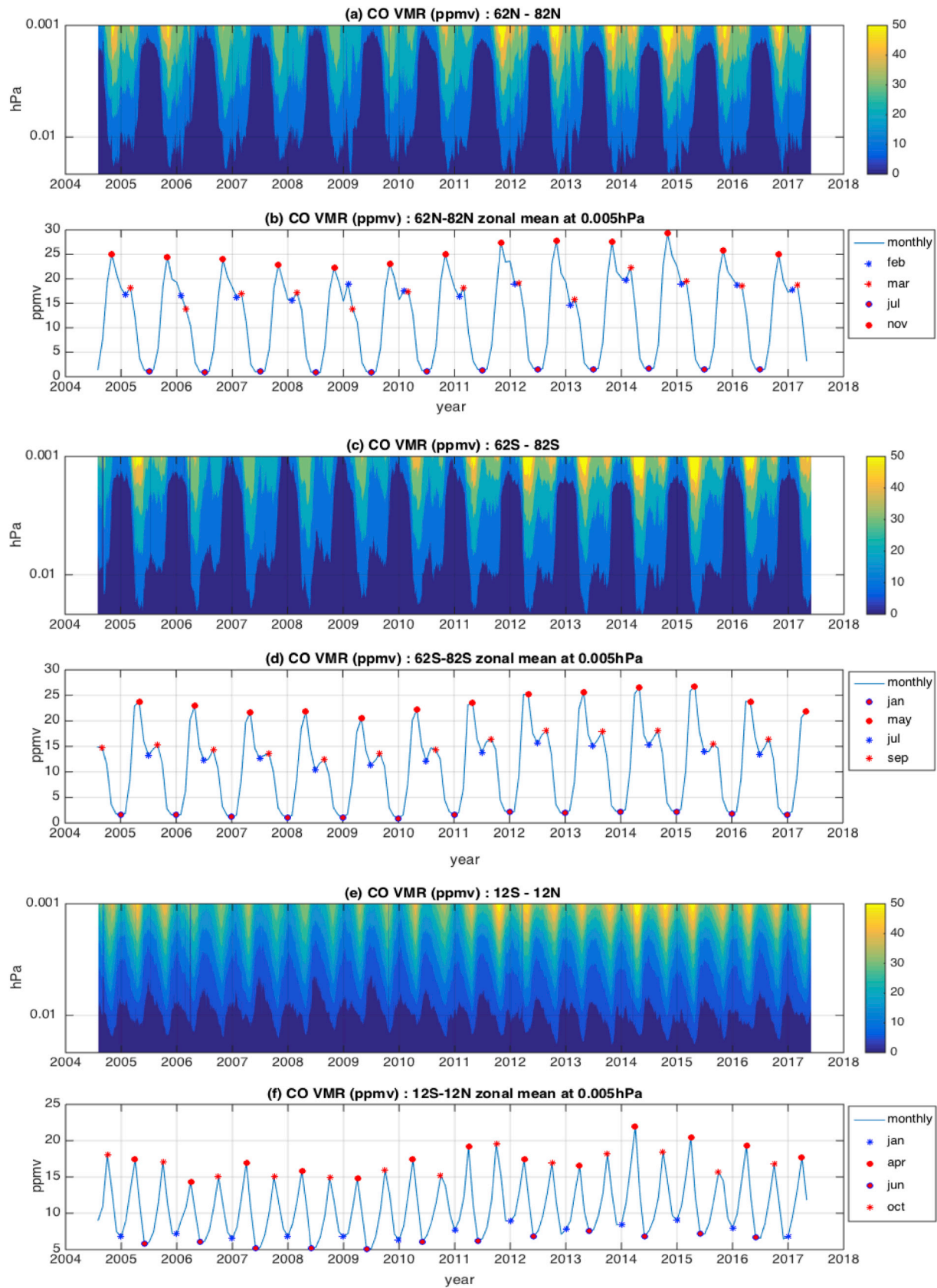


Fig. 2. MLS zonal mean CO volume mixing ratio (VMR) in ppmv during 2004–2017. (a) time-height development of CO VMR and (b) time series of CO VMR at 0.005 hPa in NH high latitude (62°N–82°N). (c) and (d), similar to (a) and (b), but in SH high latitude (62°S–82°S). (e) and (f), similar to (a) and (b), but in tropics (12°S–12°N). Markers in each line plot in (b), (d), and (f) indicate the annual and semiannual maxima and minima of the CO abundances.

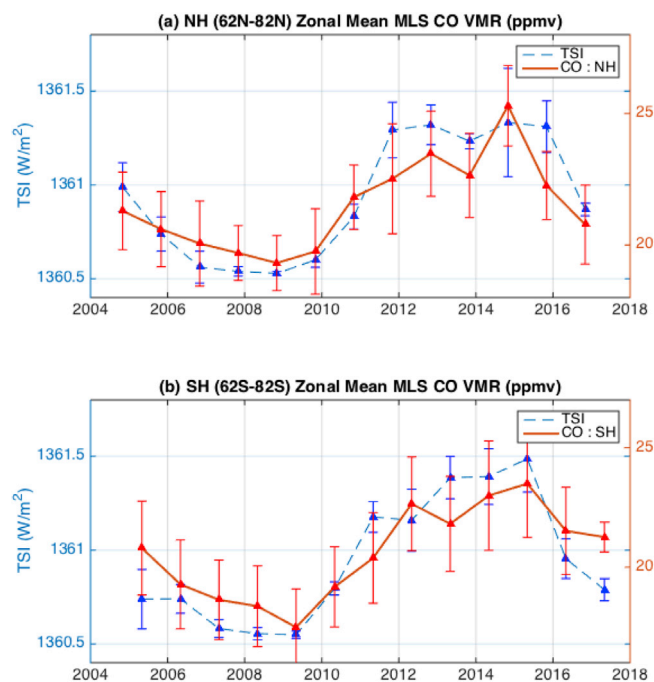


Fig. 3. High latitude (a) NH (62°N–82°N) and (b) SH (62°S–82°S) zonal mean MLS CO VMR in ppmv during early winter; from October to December for NH and from April to June for SH at 0.005 hPa. Blue dotted curves are the monthly SORCE TSI values in W/m^2 to illustrate the CO correlation with 11-year solar cycle. In both TSI and CO, the error bars indicate standard deviations of data calculated from daily zonal mean values during three months of analyzed periods. (For interpretation of the references to color in this figure legend, the reader is referred to the Web version of this article.)

latitude. The TSI was at minimum in 2009 between SC 23 and SC 24. SORCE TSI measurement showed a maximum in 2011 and 2014 with double peaks, however, this maximum amplitude was lower than those of previous maxima (Kopp and Lean, 2011). Considering these caveats, the CO measured near the maximum of SC22 by ISAMS present a reasonable agreement with that observed by MLS.

To further investigate the UV impact in CO variation, daily correlations between MLS CO and UV are shown in Fig. 4 as a function of wavelength, during the month of DJFM and JJAS. CO varies approximately linearly with changes in UV in different wavelengths. The high linear correlations between CO and solar spectrum throughout the UV region show apparent CO response to changes in solar irradiance, and also allow us to use linear regression method to estimate expected CO amount change with solar cycle. The high correlations in the austral winter extends further down to the stratosphere (lower panel) due to the CO descent inside the strong vortex in SH, while those signals in the boreal winter are limited to the upper mesosphere (upper panel).

The persistent high correlation in nearly all wavelength bands can be interpreted that the UV effect on physical CO_2 photolysis is generally persistent in all UV wavelength. The low correlations in 240–250 nm reflect the effect of the highest ozone absorption peak of the Hartley band around 250 nm (Orphal et al., 2016). Strong UV absorption by ozone molecule in the upper atmosphere may result in less UV flux changes in the upper mesosphere. The significant instrument degradation near this band around 240 nm (Marty Snow; private communication, 2017) cannot be excluded as a potential factor of the low correlation in this wavelength region.

In the lower panel of Fig. 4, the linear correlations between UV in different wavelength with reference wavelength band (250–255 nm) are estimated from SOLSTICE SSI, and from NRLSSI and SRPM 2012 (<http://www.digidyna.com/Results2010/>) models. The linear correlations are calculated from the daily spectra covering the time period 2003–2013,

2003–2013, and 1997–2009, for SOLSTICE, NRLSSI, and SRPM 2012, respectively. For SOLSTICE SSI, there are high positive correlation above 0.95 among UV at short wavelengths below ~ 240 nm. Assuming that there is no reason for the SSI to be unusual around 180 nm, the low correlation around 180 nm seems like an edge effect from measurements by the two instruments, SOLSTICE A and B, as explained in section 2.2.

This figure also illustrates an example that all SSI is in phase with each other, but the correlations from modeled SSIs differ considerably from those of SOLSTICE observation. For NRLSSI, the linear correlation is nearly one throughout the UV wavelength from 116 to 260 nm, but drops above 260 nm. For SRPM SSI, the high correlation is nearly one above 170 nm, but it shows different features in FUV regions with sharp drops related with large changes in the UV at the strong solar emission spectral lines, since SRPM covers all levels of the solar atmosphere from the photosphere to the corona (Fontenla et al., 2011).

The persistent vertical gradient in the MLS CO VMR from the mesosphere to the lower stratosphere (Fig. 5(a) and (b)) enables to trace the anomalous CO increase induced by solar variability in the stratosphere. The zonally averaged high latitude MLS CO VMRs peak in upper mesosphere and decrease with decreasing altitude. The chemical/photochemical balance between the source and the sink leads to the strong vertical gradient. Horizontal CO gradient also reflects the vertical transport of this tracer in the winter polar vortex. Furthermore, the long CO lifetime in the polar stratosphere and mesosphere during winter polar night allows to maintain these vertical and horizontal gradients throughout the winter. CO abundance is between 1 and 60 ppmv in the pressure range 0.1 hPa (~ 60 km) to 0.001 hPa (~ 95 km). In the stratosphere, it is extremely low between 100 to 1000 ppbv in the pressure range from 100 hPa (~ 20 km) to 0.1 hPa (~ 60 km).

As shown in Fig. 5(c) and (d), the solar cycle signal extends down to the mesosphere and upper stratosphere, as revealed in the correlation coefficient between MLS CO VMR and SORCE TSI for extended boreal winter (Fig. 5(c)) and austral winter (Fig. 5(d)). The extended signal is likely induced from the indirect atmospheric responses, in the form of dynamical transport, to the solar cycle driven photochemistry forcing. The maximum time lag correlations are taken as the highest correlation at each latitude and height, when the SSI time series leads with time lag between 0 and 30 days. These correlations are slightly higher than those shown in Lee13, which are calculated without time lag in the correlation analysis. Because the vertical descent is often occurring within 30 days in the mesosphere (Lee et al., 2011), the maximum correlation coefficients with lag can capture the high positive correlation between MLS CO and TSI. The correlations that are different from zero within 95% confidence levels are colored. The correlation maps show statistically significant areas over a wide region from the equator to the winter pole.

The statistically significant solar signals in CO distributions are quite symmetric in two hemispheres, while noticeable differences are evident in the downward extension of the solar signal in the December and July correlations found in Lee13. With extended analysis period for the boreal winter (DJFM, 2004–2017), the daily correlations between solar irradiance and CO are hemispherically symmetric and are more significant with extended analysis period. Strong positive correlation has the largest amplitude in the upper mesosphere (between 0.01 hPa and 0.001 hPa) throughout the equator to the high latitude of winter hemisphere. Those strong signals tend to propagate down to the upper stratosphere below 1 hPa, due to the wintertime polar descent from the upper mesosphere when the strong vortex is forming. Similarly, a strong positive correlation is shown in the SH during the austral winter (JJAS, 2004–2016) throughout the mesosphere, down to the upper stratosphere. The correlation is significant above 0.8 in the SH when the TSI is used as a solar index to compute the correlation.

As shown in Lee13, no significant negative correlation between solar irradiance and CO is found in the current analysis, confirming that an increase in the solar irradiance would be a major source of CO variance in the upper mesosphere. The solar-driven CO signals are brought downward by dynamic transports at high latitudes, causing anomalous CO

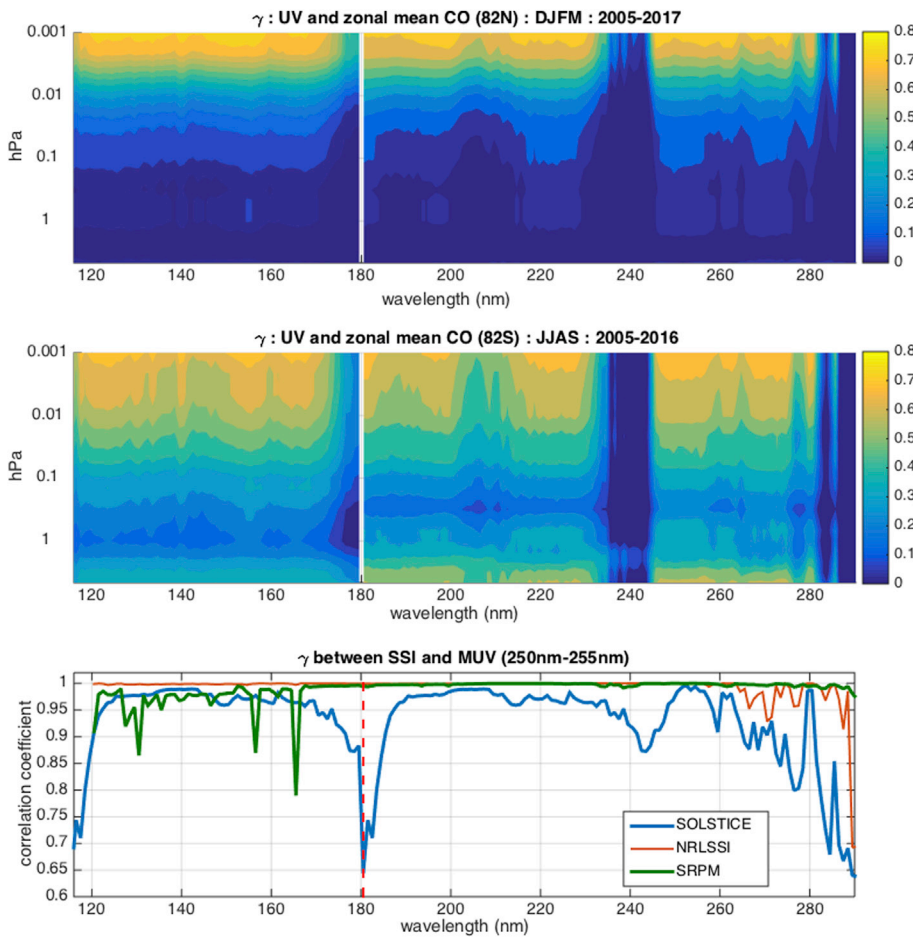


Fig. 4. Daily correlation between MLS CO and SORCE SOLSTICE UV as a function of wavelength during the month of DJFM (top), same during the month of JJAS (middle). Daily correlation between SOLSTICE UV and MUV (250–255 nm) as a function of wavelength is also shown (lower).

variations in the lower mesosphere and stratosphere. In contrast, the CO variations are weak in the summer mesosphere, mainly due to upward-directed advection.

The high linear correlations between CO, UV SSI spectrum, and TSI allow us to use linear regression method to estimate expected CO amount change with UV. To estimate the sensitivity of CO to solar cycle, we regress the CO VMR anomaly on SORCE measured MUV irradiance at 220 nm, and show it in log10 (ppmv) per % change of MUV amount. As shown in Fig. 5(e)–5(f), the maximum CO response to 1% change of MUV is as high as 1 ppmv in the upper mesosphere (above 0.005 hPa or 80 km). The sensitivity decreases in the lower mesosphere and stratosphere. Considering the MUV irradiance variance during December 2004–December 2009 is over 5% (4.85×10^{-2} to $\sim 4.63 \times 10^{-2}$ W/m²/nm), the change of winter time CO amount can be as high as ~ 5 ppmv during the same period. Similarly, MUV irradiance changed less than 3% (from 4.63×10^{-2} W/m²/nm to 4.75×10^{-2} W/m²/nm) from the minimum of SC23 (December 2009) to maximum of SC24 (December 2014). The change of winter time CO is over 3 ppmv during this period.

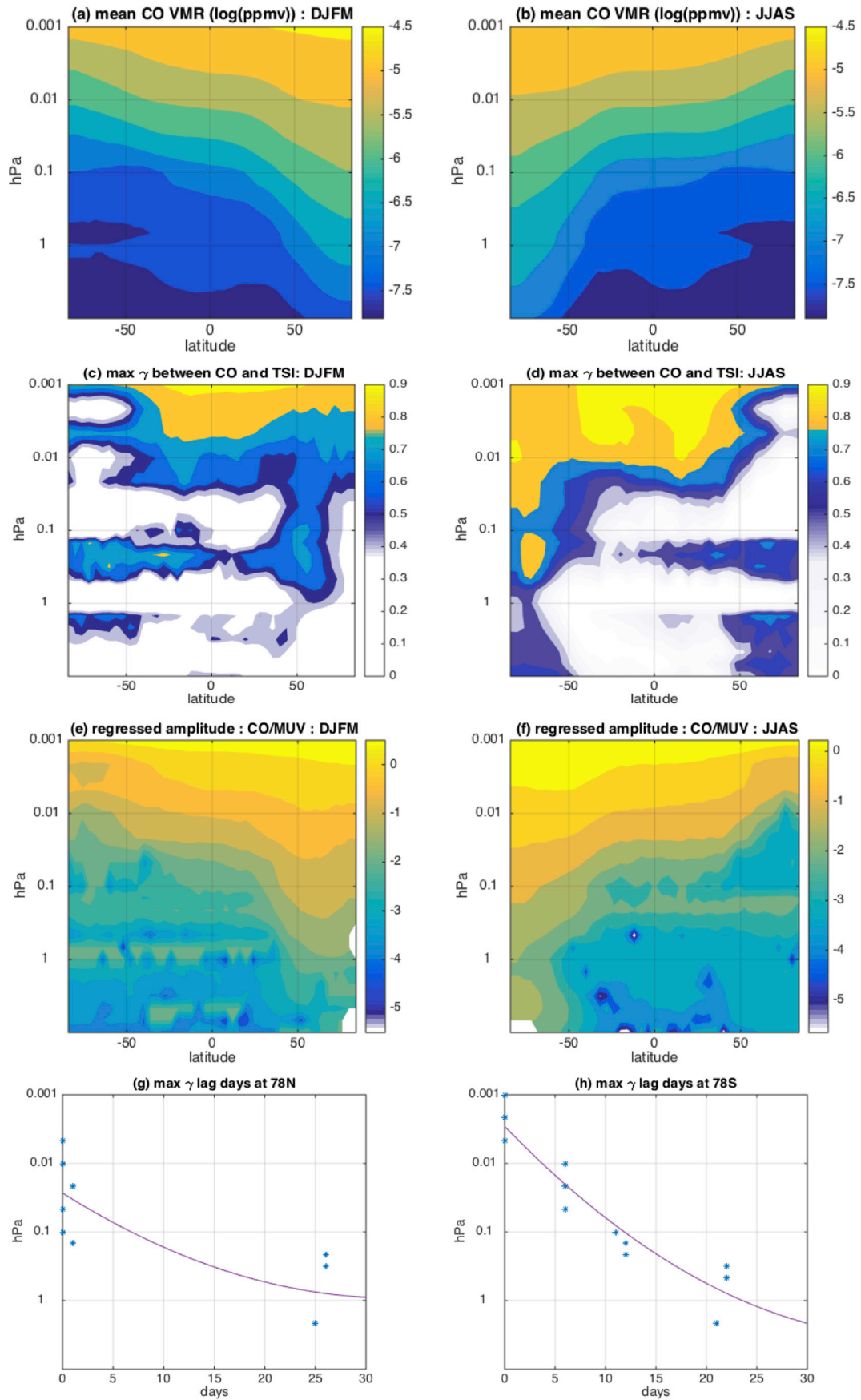
The lag correlations between FUV and CO are calculated to estimate the time delayed CO response to the instant solar forcing by the vertical transfer of the signal through the polar descent. As shown in Fig. 5(g) for 78 N and (h) for 78 S, the lag days of the maximum correlation between the CO and FUV increases from 0 day in the upper mesosphere (above 0.01 hPa) to 25 days in the upper stratosphere (1 hPa). These results suggest that solar signals in CO propagate downward from 0.001 hPa to 1 hPa within 30 days. This descent rate of the solar signal corresponds to ~ 1.3 km/day (~ 31 days from 80 to 40 km) and compares well with those estimated from the downward propagation of the maximum CO Northern Annular Mode (CNAM) and Southern Annular Mode (CSAM) index (Lee et al., 2011).

It is interesting that the lag days of maximum correlation show monotonic descent in SH, as a result of the CO descent inside the strong vortex due to a smooth evolution of polar vortex in SH. This not so smooth descent of maximum correlation lag days in the NH reflects the fact that NH polar vortex is more variable with dynamic disturbances, i.e. sudden stratospheric warmings (Limpasuvan et al., 2012).

Besides the vertical transport in the polar region, vertical mixing due to tidal and gravity wave breaking brings the CO anomaly in the lower thermosphere down to the mesosphere throughout the globe. As seen in Fig. 6, the enhanced CO anomaly in the equatorial region is indicative of strong vertical mixing due to tide waves since the diurnal tidal amplitudes normally peak semiannually around the equinoxes. On the other hand, gravity waves can also play a significant role in enhancing the vertical mixing globally as reported by previous studies (Burrage et al., 1995; McLandress, 2002; Nguyen and Palo, 2013). During the 2015 spring season, enhanced positive CO anomaly is shown in the tropics at 0.01 hPa level, indicating strong vertical mixing during that year.

As seen in Fig. 7, the distribution of CO VMR during equinox shows a quick change of meridional distribution between the month of March and April. The increased CO VMR at tropics near equator at 0.01 hPa during the month of March and April, as shown in the lower panel of Fig. 7, indicates the enhanced CO by vertical mixing due to tidal wave.

The time series of zonal mean MLS CO VMR at 0.005 hPa shows higher CO amount during high solar activity period during declining phase of SC23 (2004–2006) and SC24 maximum period (2012–2014), in both hemispheres (Fig. 8(a) and (b)). CO VMR is higher in the NH and shows more pronounced variability related to enhanced planetary wave activity. CO VMR in the SH during month of July shows intrusion of low density CO from low latitude to high latitude through meridional transport during solar minimum years. Double peaks in NH reflect double



(caption on next page)

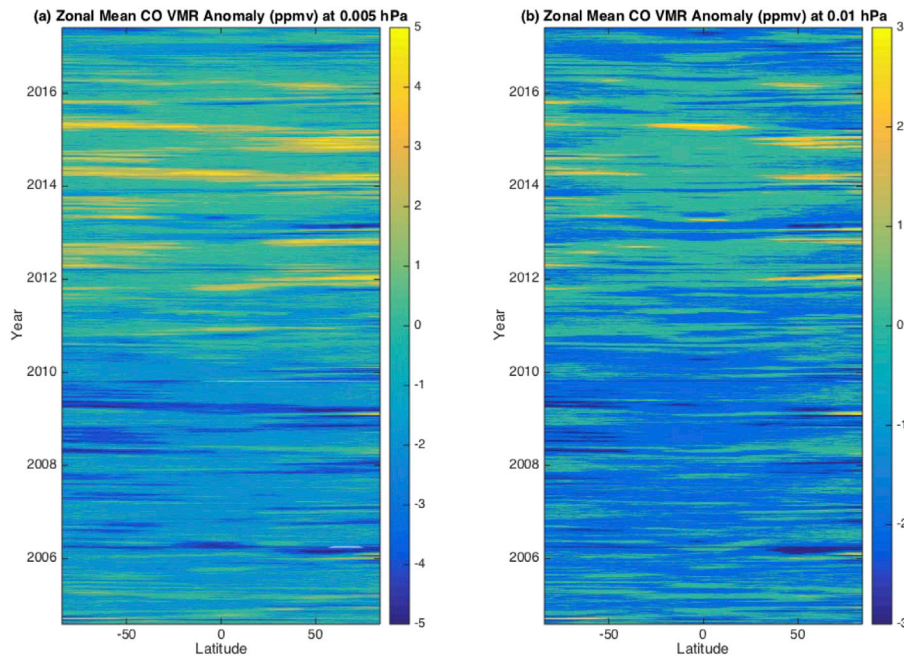


Fig. 6. Time-latitude development of (a) zonal mean CO VMR anomaly (ppmv) at 0.005 hPa and (b) zonal mean CO VMR (ppmv) at 0.01 hPa.

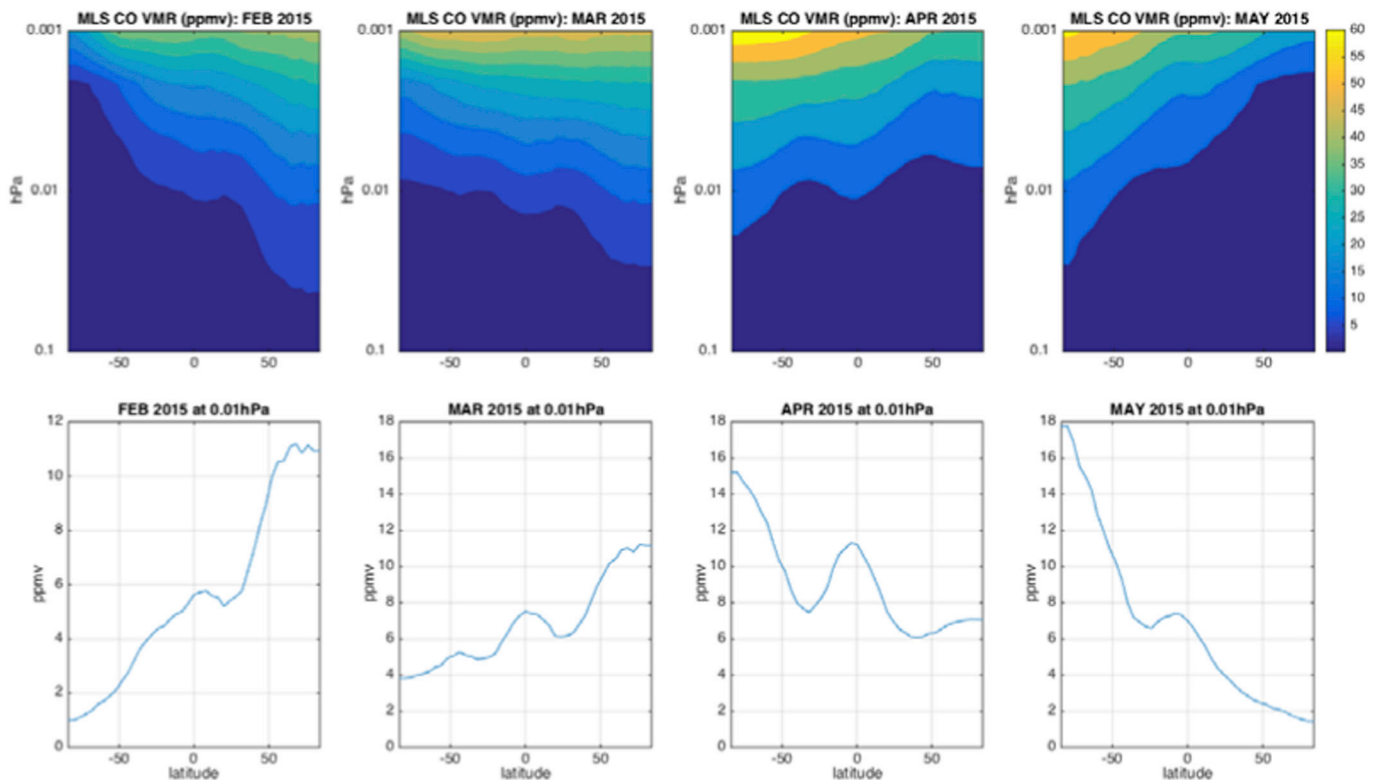


Fig. 7. MLS CO VMR (ppmv) latitude-height distribution (upper panel) and at 0.01 hPa level (lower level), during the equinox season, for February, March, April, and May 2015, respectively.

maximum of SC24 during the month of January. The solar cycle variation of CO is more prominent in the NH than in the SH, as expected due to variability induced by planetary waves.

The MLS temperature at 0.005 hPa (Fig. 8(c) and (d)) shows a large pole-to-pole gradient in temperature distribution. The summer polar mesosphere temperature is only on the order of 140 K, while that of

Fig. 5. Daily average of zonal mean MLS CO in Log_{10} (ppmv) as a function of latitude (a) for the DJFM, 2005–2017(b) for JJAS, 2005–2016. The maximum lag correlation coefficient between daily SORCE TSI and zonal mean MLS CO VMR calculated for (c) DJFM and (d) JJAS. The sensitivity of CO to the % change of FUV (in Log_{10} (ppmv) per %) estimated by regressing CO VMR on MUV (220 nm) for (e) DJFM and (f) JJAS. The lag days of maximum correlation is plotted as a function of altitude for (g) DJFM and (h) JJAS. The correlations, which are different from zero within 95% confidence levels are colored.

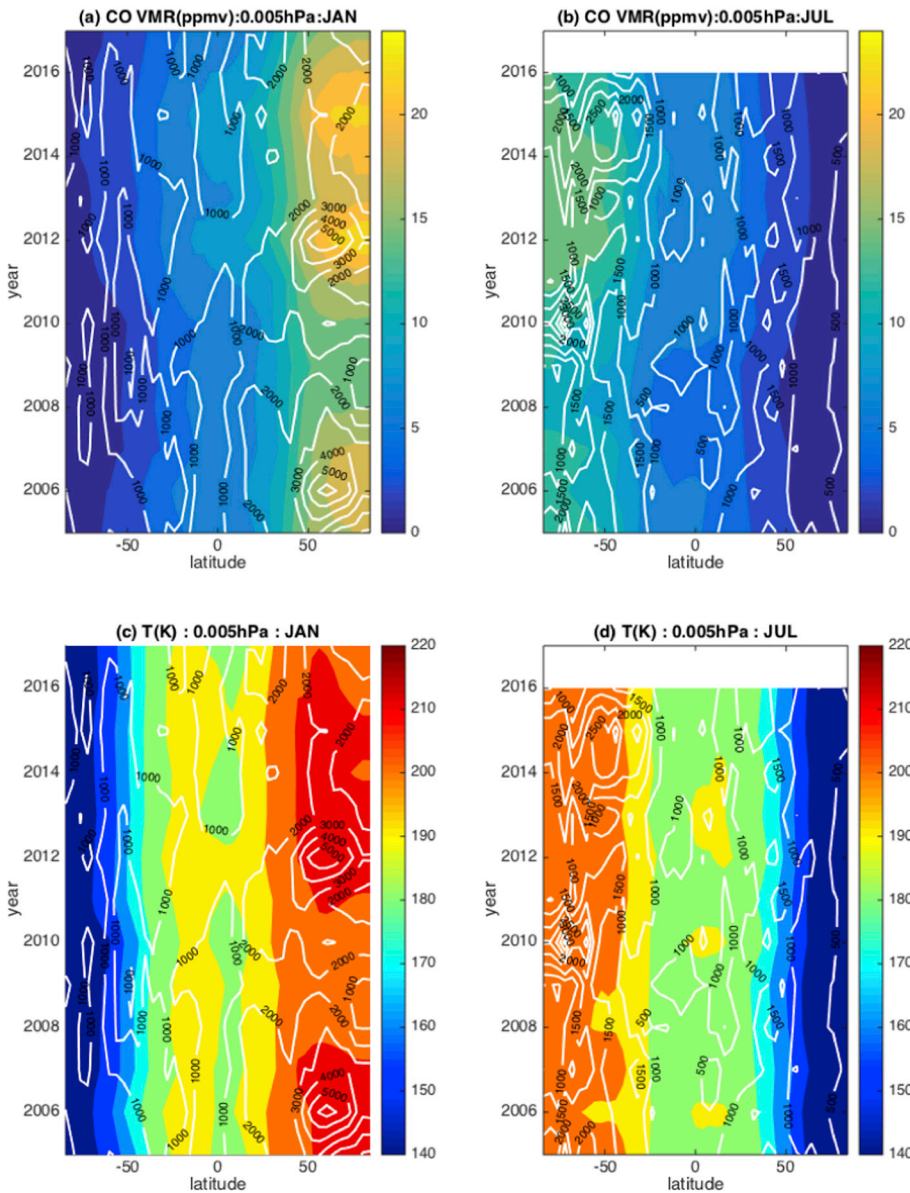


Fig. 8. Time-latitude development of (a)–(b) zonal mean CO VMR (ppmv) and (c)–(d) temperature (K) at 0.005 hPa during the month of January and July, respectively. The planetary wave amplitudes are shown in white contours.

winter mesosphere is up to 220 K. The temperature during the SC 23 maximum years (2011–2014) is ~ 10 K warmer in NH polar winter than previous years, with enhanced dynamical forcing over the warmer region, as shown by the planetary wave amplitudes.

The planetary wave amplitudes are estimated at each latitude, as the sum of amplitudes of wavenumber 1, 2, and 3 component of the meridional MLS geopotential height variations. The amplitudes of the waves are estimated by applying FFT (Fast Fourier Transform) in MLS geopotential height data. The planetary wave amplitudes (shown in white contours) are enhanced in NH high latitude region, during this solar maximum period, over the warm temperature region. The warmer temperature region during solar maximum years also indicates stronger dynamical forcing from wave breaking and hence downward motion and meridional circulation.

The relative CO variations at 0.005 hPa exhibit strong dynamical forcings during high solar activity period during declining phase of SC23 (2004–2006) and SC24 maximum period (2012–2014), in both hemispheres. These pulses exert additional CO enhancement on top of the solar cycle variation. As a result, CO can be transported toward the lower latitude, while the enhanced polar air descent is expected to bring more CO down to the mesosphere from the thermosphere.

3.3. Roles of photochemistry and dynamics

The observed solar cycle variation of CO mixing ratio in the mesosphere is induced mostly through transporting the solar modulated CO production in the thermosphere. Besides the vertical transport, solar induced CO anomaly is vertically mixed through diffusion (Solomon et al., 1985; Randel et al., 1993; Rezac et al., 2015) and hemispheric coupling (Cullens et al., 2016). However, it is not straightforward to separate photochemical and dynamical effects with the MLS data only. To separate the dynamical effect on CO variation from photochemistry driven changes, we performed a statistical experiment with a solar index.

We use the Lyman α (121.6 nm) irradiance composite as a solar index, as described in section 2.2, to represent the solar forcing to the CO photochemical processes in the mesosphere. We obtained two latitude-dependent functions, called Function1 and Function2, to characterize the CO variance in the upper mesosphere. Function1 is derived by regressing the zonal mean CO VMR to the Lyman- α index independently at each latitude. It is simply the regression coefficient at each latitude, as shown in Fig. 9(a) for January and 10(a) for July. This function captures 76%/84% of the total CO variance at 0.005 hPa for January/July and closely follows the mean CO VMR values, as expected. A Principal Component

Analysis (PCA) is applied to the residuals after the Lyman- α regression, most of which are likely driven by the variability in the lower atmosphere such as Quasi-Biennial Oscillation (QBO)-like variances. The first EOF is called Function2 in Figs. 9(b) and 10(b). The Principal Components (PCs) of the first EOFs are shown in red curves in Figs. 9(b) and 10(b). The PCs show a strong QBO-like oscillation between 2010 and 2017, which have been argued by a number of authors as a major forcing in the mesosphere (e.g., Kuchar et al., 2015; and reference therein). The residuals after the regressions account for 4% of the total variance.

Combination of Function1 and Function2 accounts for 96% and 95% of CO variance at 0.005 hPa for January and July, or 89% annually (Table 1). This annually combined percentage drops to 80% and 84% at 0.05 hPa and 0.2 hPa, respectively. Roughly speaking, Function1 and Function2 can be interpreted as the “photochemical” and “dynamical” contribution factors, whereby the “photochemical” contribution is

referred as to the CO production in the thermosphere transported down to the mesosphere. The “photochemical” contributions may contain some dynamical components if the residual circulation and mixing are modulated by the solar cycle (e.g., Cullens et al., 2016). However, the dynamical effects cannot be completely separated from the photochemical effects in the mesospheric CO analysis with this method.

At 0.005 hPa, the “photochemical” contribution explains most of the total variance, 68% of annual mean MLS CO variances, while the “dynamical” contribution accounts for 21% of those variances at 0.005 hPa. It is interesting to note that the partition between “photochemistry” and “dynamics” decreases with pressure, dropping to 39% vs. 41% at 0.05 hPa, and 24% vs. 60% at 0.2 hPa on the annual average, which is expected for more dynamical control in the CO variability at lower altitudes.

Also as indicated by the percentage in Table 1, the relative

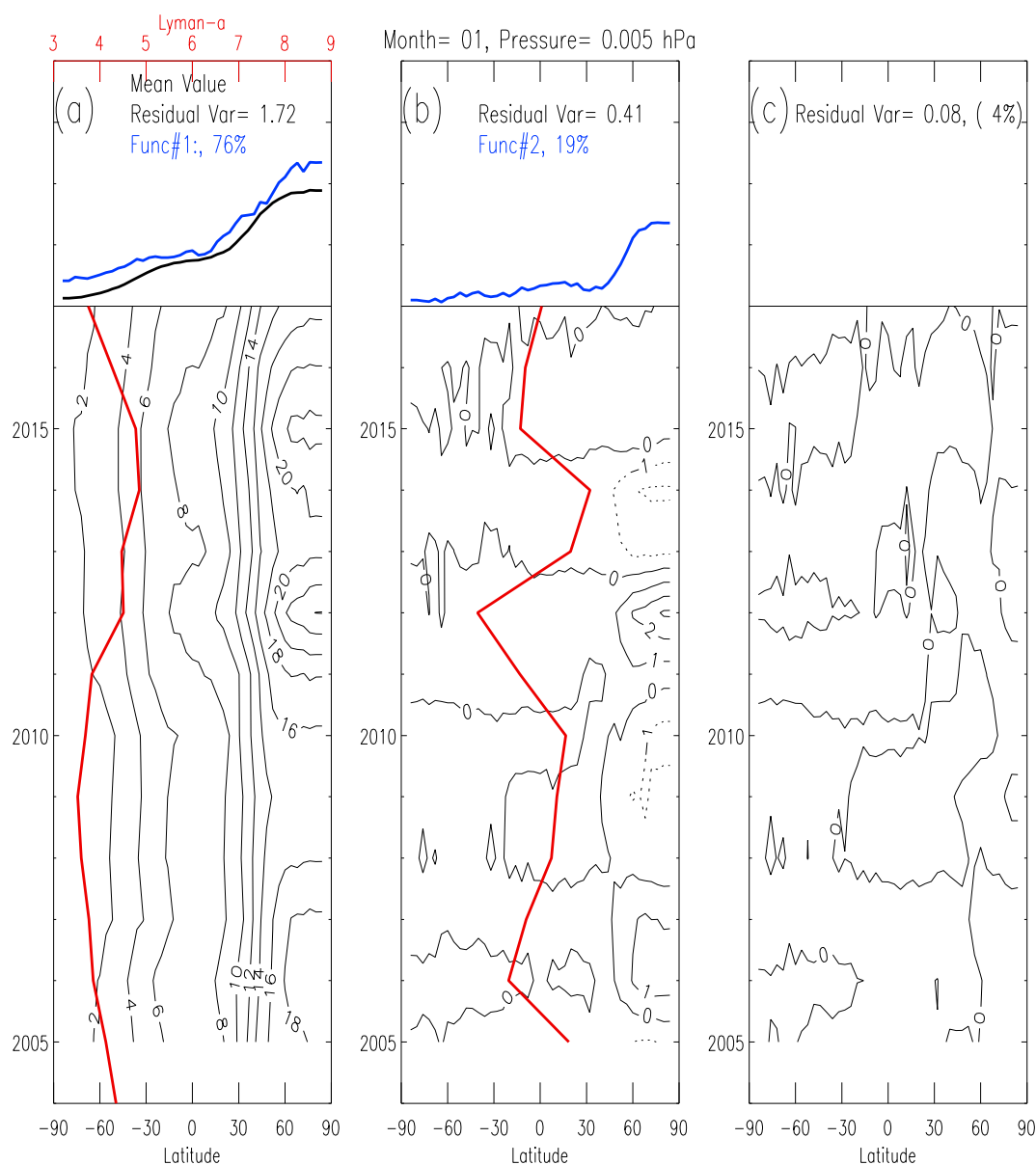


Fig. 9. (a) Time-latitude variations of January CO VMR (ppmv) at 0.005 hPa (left), (b) residuals after regressing the CO VMR in (a) to the Lyman α index, and (c) net residuals after both regression analyses in (a) and (b). The time series of Lyman α index composite (red curve) in (a) is obtained from LISIRD and has unit in 10^{11} photons/cm²/s with label in the top axis. Function 1 and 2 are shown in blue curves in the top panels. The black curve in the top panel is zonal mean of monthly CO VMR. Red curve in (b) indicates the first PC of the PCA analysis. The percentage of variance from fitting Function1 and Function2 account for 76% and 19% of the CO variance, respectively, with the remaining of 4% unexplained. (For interpretation of the references to color in this figure legend, the reader is referred to the Web version of this article.)

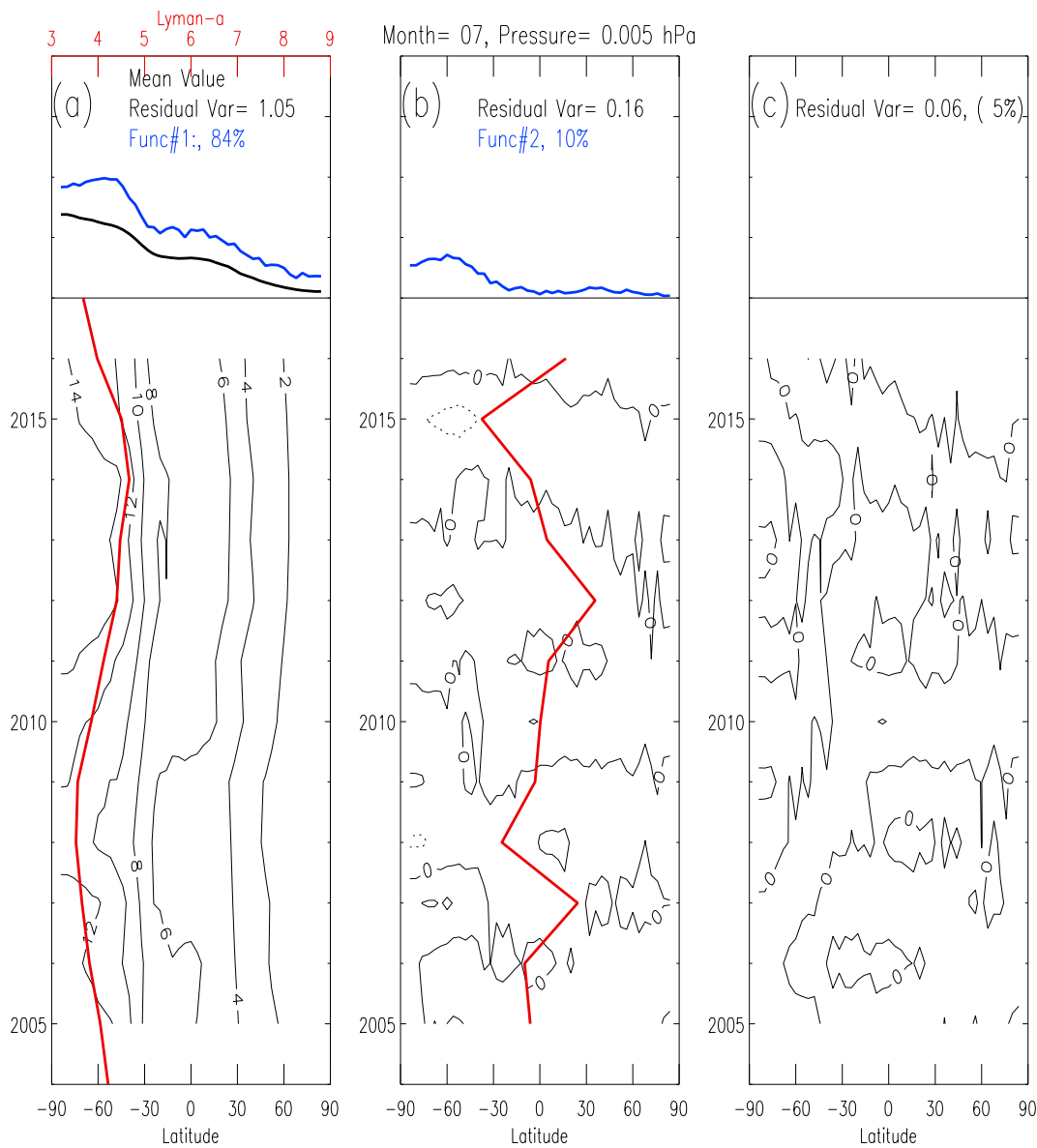


Fig. 10. As in Fig. 8, but for the month of July. The percentage of variance from fitting Function1 and Function2 account for 84% and 10% of the CO variance, respectively, with the remaining of 5% unexplained.

Table 1
Percentage of the CO variance from two function fitting.

Month	0.005 hPa			0.05 hPa			0.2 hPa		
	Func1	Func2	Res	Func1	Func2	Res	Func1	Func2	Res
Jan	76%	19%	4%	47%	31%	21%	2%	84%	12%
Feb	43%	41%	15%	2%	83%	12%	19%	76%	4%
Mar	55%	36%	8%	11%	69%	18%	17%	78%	4%
Apr	65%	16%	18%	22%	42%	34%	23%	57%	18%
May	77%	13%	9%	49%	35%	14%	44%	47%	7%
Jun	82%	11%	5%	59%	29%	10%	8%	75%	15%
Jul	84%	10%	5%	59%	24%	16%	29%	44%	26%
Aug	77%	14%	8%	55%	33%	11%	49%	38%	12%
Sep	72%	17%	10%	33%	49%	17%	12%	72%	14%
Oct	62%	23%	13%	33%	37%	29%	22%	43%	34%
Nov	70%	18%	10%	52%	31%	16%	37%	50%	12%
Dec	50%	39%	9%	43%	33%	23%	29%	54%	15%
Annual	68%	21%	11%	39%	41%	18%	24%	60%	16%

contributions from Functions 1 and 2 vary from month to month. Compared to the northern winter months, the southern winter months have a higher percentage of contributions from “photochemical” processes, since the dynamics are more variable in the northern winters. The “dynamical” contribution is particularly strong in February in the NH, when planetary wave activity and breaking are highest at high latitudes among all.

In previous work, the zonal mean CO variance in the middle atmosphere is determined as time-spatial patterns by applying PCA (Ruzmaikin et al., 2014). Both principal components show strong signals in the low thermosphere near the mesopause, and are modulated by the 11-year solar cycle. The PC1 has opposite signs in the NH and SH at mid to high latitudes and strongly oscillates with an annual periodicity. The second principal component (PC2) has the same sign in both hemispheres and oscillates mainly with a semi-annual cycle. Details in this analysis are described in Ruzmaikin et al. (2014).

3.4. CO in WACCM simulations

As described in section 2.2, the solar cycle signal in CO is further examined with a climate model experiment with WACCM by implementing fixed solar forcing based on two different modeled SSIs: SRPM 2012 and NRLSSI. The Community Earth System Model CESM1.0.3/WACCM is a full chemistry coupled global model extending from the surface to the thermosphere based on version 3 of the Community Atmosphere Model (CAM3) (Garcia et al., 2007, 2011). We performed model experiments with solar forcing based on two different SSIs, NRLSSI and SRPM 2012 SSI. In addition to these two simulations, we performed solar minimum simulation with fixed SSI for solar minimum condition, which can be used as a control run. The dominant source of atmospheric variability other than the solar forcing, i.e. QBO, can be largely removed by subtracting the control simulation from each simulation with different SSIs (Table 2). Each simulation was performed using the standard setup and codes provided by WACCM 3.5. In addition to the standard setup, three more instances were initialized introducing modifications of the initial setup obtained from different years in the standard runs. Simulations were completed for the 1955–2008 period, as indicated in the website mentioned in section 2.2.

The zonal mean CO VMR during month of December is shown for two experiments with SRPM and NRLSSI inputs, in comparison with MLS CO VMR (Fig. 11). Some aspects of the WACCM perform reasonably well. In general, the modeled vertical gradients in the CO VMR from the mesosphere to the lower stratosphere are similar to that acquired from MLS. However, the WACCM simulations underestimate the observed mean CO VMR by a factor of 3, with both SSIs, largely due to the missing EUV photolysis and ion reaction in this version of the model. The WACCM 3.5 does not employ the EUV photolysis [R2] and reaction by CO₂ with O⁺ [R3] as additional CO production mechanism in the thermosphere. The modeled CO distribution with the WACCM version 4.0 shows CO VMR in the same order of the observed CO, in comparison with the MIPAS and ACE-FTS (Garcia et al., 2014).

WACCM simulations show comparable CO VMRs with different SSIs. The amplitude of UV changes associated with 11-year solar cycle in SRPM 2012 is substantially greater than those of NRLSSI depending on wavelength (Ermolli et al., 2013). However, the modeled CO response to those two different SSIs are relatively similar to each other, when it is compared to the difference between modeled and observed CO variability, suggesting a strong dynamics control of modeled CO variability in the mesosphere.

Shown in Fig. 12 are comparisons of CO VMR (in ppmv) between simulated zonal mean CO with SRPM SSI and (a) simulated CO with NRLSSI and (b) MLS CO below 90 km, during the month of December. The modeled December CO variability in the mesosphere underestimates the observed CO by a factor of 3, suggesting the missing EUV photolysis and ion reaction mechanism, and the lack of vertical mixing in this version of the model. As a consequence, without sufficient mixing, the

Table 2

WACCM Experiment with five solar cycles (1955–2005).

Experiments	TSI	SSI (>120 nm)	SSI (<120 nm)
S_const	Constant Solar minimum	SRPM 2012	F10.7, Kp, Ap
S_srpm	Repeated Cycle 23	SRPM 2012	F10.7, Kp, Ap
S_nrl	Cycles 19–23	NRL	F10.7, Kp, Ap

simulated variations of CO are smaller than those from observation in the mesosphere. Different inputs of the solar spectrum have small impacts, not enough to explain the large discrepancy between the model and the observation.

4. Conclusions

As described in the above sections, mesospheric CO abundance and variability are determined by the lower thermospheric photochemistry and dynamical transport in the winter polar upper atmosphere. The 11-year variation in solar forcing may have direct and indirect impacts on these CO-controlling processes. MLS observations in the upper mesosphere suggest that both processes are likely modulated by the solar cycle.

1. MLS January CO variations at 0.005 hPa exhibit enhanced anomalies in 2006, 2012, and 2015 in the northern polar winter. These pulses exert additional CO enhancement on top of the solar cycle variation, more prominent in the NH than in the SH, as expected for the more variability induced by planetary waves.
2. Aura MLS monthly averaged CO over 62 N–82 N during early boreal winter (October to December) varies by about 20% over the 11-yr solar cycle. Statistically significant positive correlations up to 0.8 between CO and TSI/FUV are found in the upper polar mesosphere. The significant positive correlations are transferred down to the upper stratosphere throughout the high latitude region where the strong polar vortex is present.
3. The MLS temperature during solar maximum years (2013–2015) is warmer in the polar winter, indicating stronger dynamical forcing from wave breaking and hence stronger mean meridional circulation. As a result, the polar air descent in this particular solar maximum is expected to be stronger and brings more CO down to the mesosphere.
4. The “photochemical” contribution explains most (68% annually) of the total variance of MLS CO while the “dynamical” contribution accounts for 21% of the total variance at 0.005 hPa. However, this partition between “photochemistry” and “dynamics” decreases with height, as expected for more dynamical control in the CO variability at lower altitudes.
5. WACCM 3.5 simulations underestimate the observed CO variability by a factor of 3, due to missing EUV and ion chemistry productions in this version of the model. As a consequence, the simulated solar cycle variations of CO are also weaker than those obtained from observations in the mesosphere.

As high as 0.8, in both hemispheres, the correlation between MLS CO and the SOLARcycle UV is improved with extended analysis period, compared to the previous work. Because the solar UV spectrum is critical to the CO photolysis, it is not surprising to see a high correlation between CO and UV in most of the UV wavelength region. The observed positive correlation between UV and CO confirms that the increased solar irradiance lead to an abundant CO VMR via CO₂ photolysis throughout the upper mesosphere due to the deep-penetrating solar UV spectral forcing. Persistent correlations over the vertical layers in the mesosphere confirms again that the enhanced CO can also be transported to the lower mesosphere and upper stratosphere by dynamics through the vertical diabatic descent in the winter polar vortex, which extends the CO-TSI and CO-UV correlation to lower altitudes. The mean descent rate of the maximum correlation, estimated from the lagged CO-TSI correlation, is

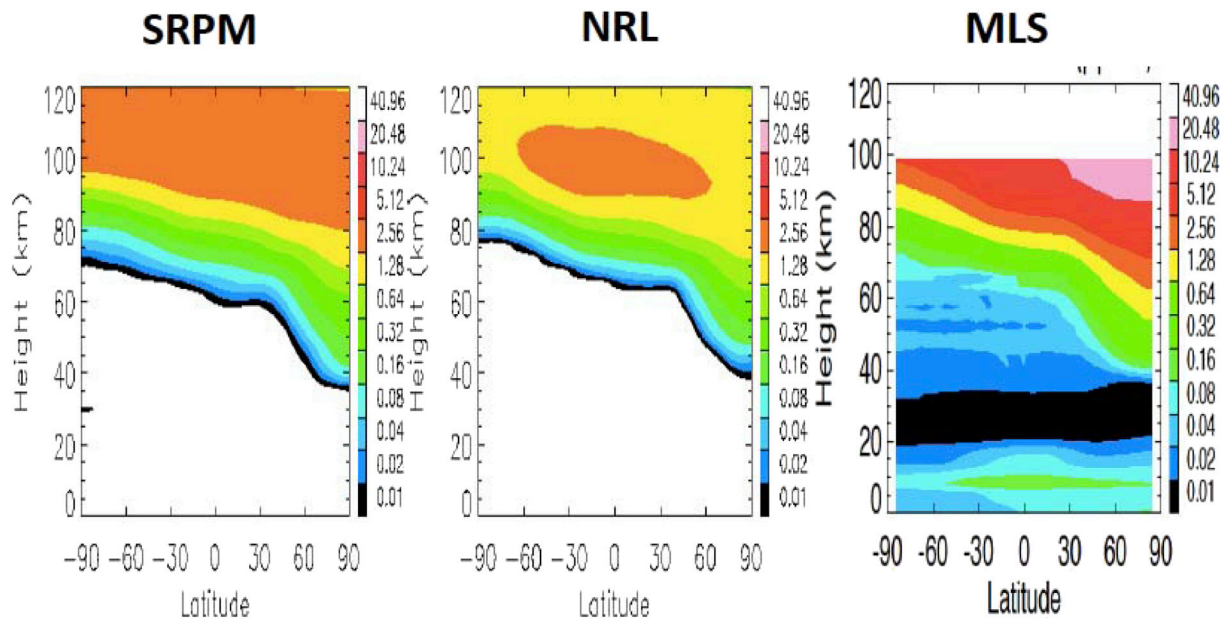


Fig. 11. WACCM simulated CO with SRPM and NRLSSI vs. MLS observed mean CO VMR (ppmv), showing that the simulated CO amounts are smaller than MLS CO in both cases.

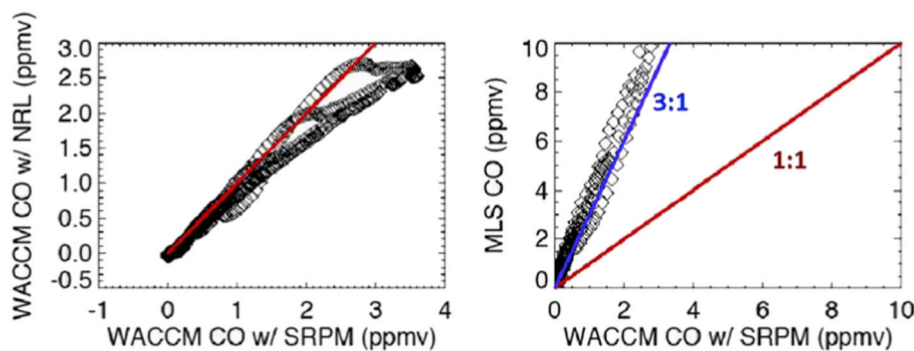


Fig. 12. WACCM simulated vs. MLS observed CO variability (ppmv) during the month of December below 90 km.

~1.3 km/day (~40 km/30 days), which is comparable with the mesospheric descent rate derived by Lee et al. (2011).

It is also worth to note that the long life-time of CO suggests that enhanced CO anomaly is redistributed globally before the CO is destroyed. The photochemistry driven CO anomaly signal is further extended in the tropics by vertical mixing. Vertical mixing by tides or gravity waves is most likely responsible for the observed extra-polar CO anomaly patterns rather than horizontal transport by the meridional circulation and inter-hemispheric coupling.

The solar cycle variation of SSI, including UV, is essential to elucidate the underlying wavelength dependent mechanisms of terrestrial interactions with the Sun. In particular, reliable long term UV data is a key element in characterizing the long-term changes of atmospheric constituents, i.e., ozone and water vapor. For a successful assessment of Earth's climate change due to solar forcing, the absolutely calibrated satellite measurements of spectral solar irradiance are vital to be used as climate model inputs, since most of the climate models depend so far on solar proxies or modeled solar spectrum.

The Total and Spectral Solar Irradiance Sensor (TSIS-1) is deployed the TIM and Spectral Irradiance Monitor (SIM) on the International Space Station in late 2017, to continue the TSI and SSI observations (200–2400 nm). The value of the long term solar total and spectral irradiance measurements, along with the fundamental middle atmosphere

measurements cannot be overemphasized.

Acknowledgments

This work is supported by NASA Sun-climate research at Goddard Space Flight Center. We would like to thank two anonymous reviewers for valuable comments and suggestions that led to an improved manuscript. We thank the Aura MLS, SORCE, NRLSSI teams for providing their data support, and Jerry Harder and Marty Snow for valuable science discussions.

References

- Allen, D.R., Stanford, J.L., Nakamura, N., Lopez-Valverde, M.A., Lopez-Puertas, M., Taylor, F.W., Remedios, J.J., 2000. Antarctic polar descent and planetary wave activity observed in ISAMS CO from April to July 1992. *Geophys. Res. Lett.* 27, 665–668.
- Angell, J.K., Korshover, J., 1981. Comparison between sea surface temperature in the equatorial eastern Pacific and United States surface temperature. *J. Appl. Meteorol.* 20, 1105–1110.
- Bates, D.R., Witherspoon, A.E., 1951. The photo-chemistry of some minor constituents of the Earth's atmosphere. *Mon. Not. Roy. Astron. Soc.* 112, 101.
- Brasseur, G.P., Solomon, S., 2005. *Aeronomy of the Middle Atmosphere*, third ed. Springer, Dordrecht, The Netherlands, pp. 1–646.

- Burrage, M.D., Hagan, M.E., Skinner, W.R., Wu, D.L., Hays, P.B., 1995. Long-term variability in the solar diurnal tide observed by HRDI and simulated by the GSWM. *Geophys. Res. Lett.* 22 (19), 2641–2644. <https://doi.org/10.1029/95GL02635>.
- Cullens, C.Y., England, S.L., Garcia, R.R., 2016. The 11 year solar cycle signature on wave-driven dynamics in WACCM. *J. Geophys. Res. Space Physics* 121, 3484–3496. <https://doi.org/10.1002/2016JA022455>.
- Ermolli, I., Matthes, K., Dudok de Wit, T., Krivova, N.A., Tourpali, K., Weber, M., Unruh, Y.C., Gray, L., Langematz, U., Pilewskie, P., Rozanov, E., Schmutz, W., Shapiro, A., Solanki, S.K., Woods, T.N., 2013. Recent variability of the solar spectral irradiance and its impact on climate modeling. *Atmos. Chem. Phys.* 13, 3945–3977. <https://doi.org/10.5194/acp-13-3945-2013>.
- Fontenla, J.M., Curdt, W., Haberleiter, M., Harder, J., Tian, H., 2009. Semiempirical models of the solar atmosphere. III. Set of non-LTE models for far-ultraviolet/extreme-ultraviolet irradiance computation. *Astrophys. J.* 707, 482–502. <https://doi.org/10.1088/0004-637X/707/1/482>.
- Fontenla, J.M., Harder, J., Livingston, W., Snow, M., Woods, T., 2011. High-resolution solar spectral irradiance from extreme ultraviolet to far infrared. *J. Geophys. Res.* 116, D20108 <https://doi.org/10.1029/2011JD016032>.
- Funke, B., et al., 2009. Carbon monoxide distributions from the upper troposphere to the mesosphere inferred from 4.7 μm non-local thermal equilibrium emissions measured by MIPAS on ENVISAT. *Atmos. Chem. Phys.* 9 (7), 2387–2411.
- Garcia, R.R., Marsh, D.R., Kinnison, D.E., Boville, B.A., Sassi, F., 2007. Simulation of secular trends in the middle atmosphere, 1950–2003. *J. Geophys. Res.* 112, D09301 <https://doi.org/10.1029/2006JD007485>.
- Garcia, R.R., Randel, W.J., Kinnison, D.E., 2011. On the determination of age of air trends from atmospheric trace species. *J. Atmos. Sci.* 68, 139–154.
- Garcia, R.R., Lopez-Puertas, M., Funke, B., Marsh, D.R., Kinnison, D.E., Smith, A.K., 2014. On the distribution of CO₂ and CO in the mesosphere and thermosphere. *J. Geophys. Res.* 119, 5700–5718. <https://doi.org/10.1002/2013JD021208>.
- Kopp, G., Lawrence, G., 2005. The total irradiance monitor (TIM): instrument design. *Sol. Phys.* 230, 1–2. <https://doi.org/10.1007/s11207-005-7446-4>.
- Kopp, G., Heuerman, K., Lawrence, G., 2005. The total irradiance monitor (TIM): instrument calibration. *Sol. Phys.* 230, 111–127. <https://doi.org/10.1007/s11207-005-7447-3>.
- Kopp, G., Lean, J.L., 2011. A new, lower value of total solar irradiance: evidence and climate significance. *Geophys. Res. Lett.* 38, L01706 <https://doi.org/10.1029/2010GL045777>.
- Kuchar, A., Sacha, P., Miksovsky, J., Pisoft, P., 2015. Solar cycle in current reanalyses: (non)linear attribution study. *Atmos. Chem. Phys.* 15, 6879–6895. <https://doi.org/10.5194/acp-15-6879-2015>.
- Lean, J.L., 1997. The Sun's variable radiation and its relevance for Earth. *Annu. Rev. Astron. Astrophys.* 35, 33–67. <https://doi.org/10.1146/annurev.astro.35.1.33>.
- Lean, J.L., 2000. Evolution of the Sun's spectral irradiance since the maunders minimum. *Geophys. Res. Lett.* 27, 2425–2428. <https://doi.org/10.1029/2000GL000043>.
- Lee, J.N., Wu, D.L., Manney, G.L., Schwartz, M.J., Lambert, A., Livesey, N.J., Minschwaner, K.R., Pumphrey, H.C., Read, W.G., 2011. Aura Microwave Limb Sounder observations of the polar middle atmosphere: dynamics and transport of CO and H₂O. *J. Geophys. Res.* 116, D05110 <https://doi.org/10.1029/2010JD014608>.
- Lee, J.N., Wu, D., Ruzmaikin, A., 2013. Interannual variations of MLS carbon monoxide induced by solar cycle. *J. Atmos. Sol. Terr. Phys.* 102, 99–104. <https://doi.org/10.1016/j.jastp.2013.05.012>.
- Limpasuvan, V., Richter, J.H., Orsolini, Y.J., Stordal, F., Kvissel, O.-K., 2012. The roles of planetary and gravity waves during a major stratospheric sudden warming as characterized by WACCM. *J. Atmos. Sol. Terr. Phys.* 78–79, 84–98. <https://doi.org/10.1016/j.jastp.2011.03.004>.
- López-Valverde, M.A., López-Puertas, M., Remedios, J.J., Rodgers, C.D., Taylor, F.W., Zipf, E.C., Erdman, P.W., 1996. Validation of measurements of carbon monoxide from the improved stratospheric and mesospheric sounder. *J. Geophys. Res.* 101 (D6), 9929–9955. <https://doi.org/10.1029/95JD01715>.
- McClintock, W.E., Rottman, G., Woods, T.N., 2005a. Solar-stellar irradiance comparison experiment II (SOLSTICE II): instrument concept and design. *Sol. Phys.* 230, 225.
- McClintock, W.E., Snow, M., Woods, T.N., 2005b. Solar-stellar irradiance comparison experiment II (SOLSTICE II): pre-launch and on-orbit calibrations. *Sol. Phys.* 230, 259.
- McLandress, C., 2002. Interannual variations of the diurnal tide in the mesosphere induced by a zonal-mean wind oscillation in the tropics. *Geophys. Res. Lett.* 29, 1944–8007. <https://doi.org/10.1029/2001GL014551>.
- Minschwaner, K., et al., 2010. The photochemistry of carbon monoxide in the stratosphere and mesosphere evaluated from observations by the Microwave Limb Sounder on the Aura satellite. *J. Geophys. Res.* 115, D13303 <https://doi.org/10.1029/2009JD012654>.
- Nguyen, V., Palo, S., 2013. Technique to produce daily estimates of the migrating diurnal tide using TIMED/SABER and EOS Aura/MLS. *J. Atmos. Sol. Terr. Phys.* 105–106, 39–53. <https://doi.org/10.1016/j.jastp.2013.07.008>.
- Orphal, J., et al., 2016. Absorption cross-sections of ozone in the ultraviolet and visible spectral regions: status report 2015. *J. Mol. Spectrosc.* 327, 105. <https://doi.org/10.1016/j.jms.2016.07.007>.
- Parkinson, W.H., Rufus, J., Yoshino, K., 2003. Absolute absorption cross section measurements of CO₂ in the wavelength region 163–200 nm and the temperature dependence. *Chem. Phys.* 290, 251–256.
- Pilewskie, P., Rottman, G., Richard, E., 2005. An overview of the disposition of solar radiation in the lower atmosphere: connections to the SORCE mission and climate change. *Sol. Phys.* 230 (1), 55–69.
- Pumphrey, H.C., et al., 2007. Validation of middle-atmosphere carbon monoxide retrievals from the Microwave Limb sounder on Aura. *J. Geophys. Res.* 112, D24S38 <https://doi.org/10.1029/2007JD008723>.
- Qian, L., Solomon, S.C., Kane, T.J., 2009. Seasonal variation of thermospheric density and composition. *J. Geophys. Res.* 114, A01312 <https://doi.org/10.1029/2008JA013643>.
- Randel, W.J., Gille, J.C., Roche, A.E., Kumer, J.B., Mergenthaler, J.L., Waters, J.W., Fishbein, E.F., Lahoz, W.A., 1993. Stratospheric transport from tropics to middle latitudes by planetary wave mixing. *Nature* 365, 533–535.
- Rezac, L., Jian, Y., Yue, J., Russell III, J.M., Kutepov, A., Garcia, R., Walker, K., Bernath, P., 2015. Validation of the global distribution of CO₂ volume mixing ratio in the mesosphere and lower thermosphere from SABER. *J. Geophys. Res. Atmos.* 120, 12067–12081. <https://doi.org/10.1002/2015JD023955>.
- Rottman, G., 2005. The SORCE mission. *Sol. Phys.* 230 (1), 7–25.
- Ruzmaikin, A., Lee, J.N., Wu, D.L., 2014. Patterns of carbon monoxide in the middle atmosphere and effects of solar variability. *Adv. Space Res.* 54, 320–326.
- Ryan, N.J., Kinnison, D.E., Garcia, R.R., Hoffmann, C.G., Palm, M., Raffalski, U., Notholt, J., 2018. Assessing the ability to derive rates of polar middle-atmospheric descent using trace gas measurements from remote sensors. *Atmos. Chem. Phys.* 18, 1457–1474. <https://doi.org/10.5194/acp-18-1457-2018>.
- Snow, M., McClintock, W.E., Rottman, G., Woods, T.N., 2005. Solar-stellar irradiance comparison experiment II (SOLSTICE II): examination of the solar stellar comparison technique. *Sol. Phys.* 230, 295.
- Solomon, S., et al., 1985. Photochemistry and transport of carbon monoxide in the middle atmosphere. *J. Atmos. Sci.* 42, 1072–1083, 1985.
- Waldteufel, P., 1970. A study of seasonal changes in the lower thermosphere and their implications. *Planet. Space Sci.* 18 (5), 741–748. [https://doi.org/10.1016/0032-0633\(70\)90055-3](https://doi.org/10.1016/0032-0633(70)90055-3).
- Woods, T.N., Tobiska, W.K., Rottman, G.J., Worden, J.R., 2000. Improved solar Lyman alpha irradiance modeling from 1947 through 1999 based on UARS Observations. *J. Geophys. Res.* 105, 27195–27215.
- Yoshino, K., Esmond, J.R., Sun, Y., Parkinson, W.H., Ito, K., Matsui, T., 1996. Absorption cross section measurements of carbon dioxide in the wavelength region 118.7–175.5 nm and the temperature dependence. *J. Quant. Spectrosc. Radiat. Transfer* 55, 53.